Batchelor *et al. Fire Ecology* (2025) 21:39
https://doi.org/10.1186/s42408-025-00375-2

Fire Ecology

Association for Fire Ecology

ORIGINAL RESEARCH

Open Access

Drone-based, multispectral photogrammetric point clouds to classify fire severity at differing canopy height strata

Jonathan L. Batchelor[1*], Andrew T. Hudak[2*], Akira Kato[3], David R. Weise[4] and L. Monika Moskal[1]

Abstract

Background Remote sensing techniques for assessing fire severity using two-dimensional imagery, such as satellite data, are limited to a single severity value per pixel, typically at a 30-m resolution. This often leads to an underestimation of understory fire severity, as live tree crowns can obscure the extent of the burned area beneath. By leveraging the three-dimensional capabilities of drone imagery, a more comprehensive assessment of fire severity across different canopy height strata can be achieved.

Methods We show how drone digital aerial photogrammetry (dDAP), also known as structure from motion, can be used to generate three-dimensional multispectral photogrammetric point clouds for quantifying fire effects at various canopy height strata as well as classify ground cover below normally occluding overstory trees. Conducted during prescribed fires at Fort Jackson, South Carolina, RGB and multispectral imagery were collected via drone both pre- and post-fire at five plots, with two additional unburned plots flown to serve as controls. Multispectral photogrammetric point clouds were generated and NDVI values were calculated for each point. Point clouds were segmented into 2-m height stratum layers, to compare NDVI values for different canopy height strata pre- and post-fire. Orthoimages of the understory, overstory, and traditional nadir views were generated.

Conclusions Findings showed that prescribed fire had a substantial effect on NDVI values up to 6 m in height, with only minor effects observed above 6 m. Ground cover under the canopy, typically occluded from overhead imagery, was classified with 87% accuracy. This study demonstrated the ability to digitally remove occluding tall vegetation using dDAP and to derive a more precise assessment of fire effects on ground and understory vegetation compared to two-dimensional satellite imagery.

Keywords Drone, UAV, Satellite burn indices, Fire, Photogrammetry, Multispectral, NDVI, Understory, Fort Jackson, Structure from motion

Resumen

Antecedentes El uso de técnicas de sensores remotos para determinar la severidad de los incendios mediante imágenes bidimensionales, tales como los datos de satélites, están limitadas a un solo valor de severidad por cada píxel, típicamente en una resolución de 30 m. Esto conlleva frecuentemente a una subestimación de la severidad en el sotobosque, dado que las copas vivas pueden ocultar la extensión de área quemada por debajo de las mismas.

*Correspondence:
Jonathan L. Batchelor
jonbatch@uw.edu
Andrew T. Hudak
andrew.hudak@usda.gov
Full list of author information is available at the end of the article

Mediante la potenciación de las capacidades tridimensionales de las imágenes de drones, se puede alcanzar una mayor comprensión en la determinación de la severidad del fuego a través de diferentes alturas del dosel. En este trabajo metodológico, mostramos cómo la fotogrametría aérea digital de drones (dDAP), también conocida como estructura desde el movimiento, puede ser usada para generar nubes de puntos fotogramétricos multi-espectrales tridimensionales, para cuantificar los efectos del fuego en estratos del dosel a diferentes alturas y también para clasificar la cobertura del suelo ocluidos normalmente por estos doseles. Conducidas durante quemas prescriptas en Fort Jackson, Carolina del Sur, RBG e imágenes multi-espectrales fueron colectadas vía drones tanto antes como después de las quemas en cinco parcelas, con otras dos parcelas adicionales que fueron sobrevoladas y que sirvieron como control. Se generaron nubes de puntos fotogramétricos multi-espectrales tridimensionales y se calcularon los índices de NDVI para cada punto generado. Los puntos de nubes fueron segmentados en estratos cada dos metros para comparar los valores de NDVI para las diferentes alturas de los estratos en la pre y la post quema. Se generaron luego ortoimágenes del sotobosque, del dosel, y las tradicionales vistas del nadir.

Resultados Los resultados muestran que las quemas prescriptas tienen un efecto substancial en los valores del NDVI hasta los 6 m en altura, con sólo efectos menores observados por encima de esta altura. La cobertura del suelo por debajo de los doseles, típicamente ocluida en imágenes tomadas desde arriba, fue clasificada como con una exactitud del 87%.

Conclusiones Este estudio demostró la habilidad de remover digitalmente la vegetación alta de los doseles usando dDAP, y derivar asimismo una determinación más precisa de los efectos del fuego en el suelo y en la vegetación del sotobosque comparado con las imágenes satelitales bidimensionales provistas por los satélites.

Introduction

Fire severity and its effects on vegetation differ spatially across burns, both horizontally and vertically (Agee 1996; Bessie and Johnson 1995; Rothermel 1991; Wagner 1977). Fire effects quantified at the landscape level generally rely on satellite imagery consisting of only two-dimensional (2D), nadir imagery (Szpakowski and Jensen 2019). Such images are very effective for detecting changes in overstory vegetation after a fire disturbance (Kane et al. 2013; Lydersen et al. 2016); however, changes in the understory may be difficult to detect, as the upper canopy can partially or totally occlude the understory vegetation. This is problematic because a fast-moving, low-intensity fire can remove all surface vegetation, leaving the upper canopy undamaged (Wade and Johansen 1986; Wright and Agee 2004). In areas of high-severity crown fires, there may be little to no occlusion of the ground post-fire, but in areas that have experienced a surface fire that did not move into the canopy, the live crown foliage can mask the severity on the understory if using spectral indices to quantify severity that rely on nadir imagery (Miller et al. 2009). Topography, moisture, wind patterns, and vegetation distribution are some of the factors that can lead to mixed-severity fires (Perry et al. 2011). In such fire mosaics, differentiating ground surface fire severity compared to crown severity could enable a much more accurate assessment of overall fire severity.

To derive fire severity estimates that incorporate vertical strata conditions (i.e., adding a third dimension), visual assessments of field plots are typically performed. The composite burn index is a field method that uses height strata to evaluate fire effects (Key and Benson 2006; Saberi et al. 2022). However, field sampling techniques still rely on subjective assessment and on generalizing conditions spatially, both horizontally and vertically. Much work has been done to model field indices of fire severity such as the CBI from satellite imagery (Amroussia et al., 2023; Parks et al. 2019) as well as create 3D severity metrics from aerial laser scanning (ALS). ALS has been used to quantify three-dimensional forest structure changes caused by fire and relate them to both satellite and drone imagery (Filippelli et al. 2019; Kato et al. 2019; McCarley et al. 2017; Viana-Soto et al. 2022). In areas where ALS is acquired both before and after a fire, fire severity can be quantified by the change in aboveground point distributions (Hoe et al. 2018). Although more limited in spatial coverage, Terrestrial Laser Scanning (TLS) can also be employed to quantify fire severity at strata of different heights based on point distributions (Kato et al. 2019). However, lidar with sufficient temporal resolution to be used to define severity is rare.

The concept of "severity" in the context of fire is often determined by the temporal and spatial scales at which fire effects are observed, as well as the methodologies employed to quantify these effects (Keeley 2009). Severity can be assessed through imagery by measuring changes in spectral indices such as the Normalized Differenced Vegetation Index (NDVI) or the Normalized Burn Ratio (NBR) (Escuin et al., 2008). Additionally, severity can be evaluated through field-based observations, including the consumption and charring of trees from the ground up (Key and Benson 2006). In this study, severity is defined as an immediate change in NDVI within a three-dimensional model of differenced NDVI values at various canopy heights, facilitated by the utilization of multispectral photogrammetric point clouds derived from drone imagery.

Drone digital aerial photogrammetry (dDAP)

Digital aerial photogrammetry (often called structure from motion, SfM) is used to create photogrammetric point clouds and orthoimagery mosaics from a collection of overhead images. With the increasing availability of consumer drones and processing software, drone imagery has become a staple in ecological monitoring (Colomina and Molina 2014; Hardin and Hardin 2010; Sun et al. 2021). In addition to traditional RGB imagery, drones with multispectral cameras are now employed to rapidly assess vegetation health and conditions (Fawcett et al. 2020).

Photogrammetric point clouds generated from RGB or multispectral imagery preserve the spectral reflectance values of each imagery band for each point created. Point clouds derived from 4-band multispectral imagery with near-infrared (NIR) allow for the creation of not only multispectral point clouds, but also point clouds of spectral indices such as NDVI (Reilly et al. 2021). Applications of these multispectral point clouds to address ecological questions is the subject of several papers looking at fuel estimates and forest structural attributes (Hoffrén et al. 2023; Shen et al. 2019). However a limitation of photogrammetric point clouds is that they model the surface of a forest and in areas of closed canopy, they are not able to effectively model the ground (Cao et al. 2019; Iglhaut et al. 2019).

Forested ecosystems with short fire return intervals, such as longleaf pine (*Pinus palustris* Mill.) forests in the southern US, tend to have a relatively open canopy (Beaty and Taylor 2001; Cary 1932; Landers 1991). An open canopy allows oblique angles from a drone-mounted aerial camera to capture tree stems, understory vegetation, and ground cover (Fig. 1). These oblique angles allow for a much more complete three-dimensional model of an area, including the ground and surface vegetation, even under tree canopies that would occlude nadir-only imagery. Because photogrammetric point clouds are generated from a multitude of images, what may be obscured in one image could be visible in another. Specifically, a nadir image directly above a tree will have all the ground under the tree canopy obscured, however, the photos taken in the area surrounding the tree may capture the ground (Fig. 1). With sufficient overlap between photos, it is possible to generate three-dimensional multispectral point clouds as well as an orthoimage that focuses solely on the surface vegetation, effectively excluding all tall vegetation from the image.

Pre-fire orthoimagery of the understory only, with all trees digitally removed from the point clouds before rendering rasters from the multispectral points, should allow for complete characterization of ground cover into categories such as fine vs coarse downed woody debris, bare soil, duff, low vegetation (e.g., grasses, forbs, and small shrubs), and taller understory vegetation (e.g., shrubs and saplings). Post-fire orthoimagery of the understory only, should allow for the same characterization of fuels

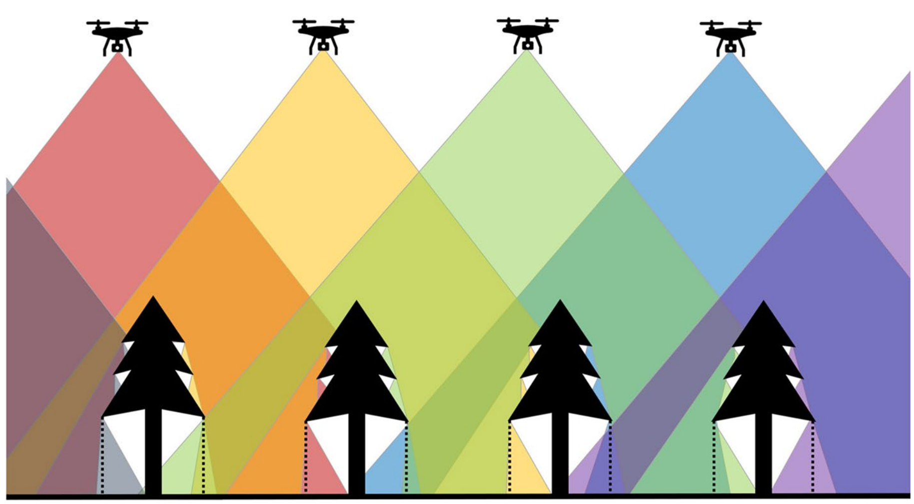

Fig. 1 Conceptual diagram of the area occluded from nadir imagery (denoted by the dashed black line). In this diagram, approximately 50% of the ground is occluded by the trees, but the entire ground is captured from the oblique views from the drones. The field of view from the drones is ~80° with ~80% overlap. These are common values for drone image acquisition

and enable a detailed quantification of the type of fuels consumed and the total consumption. How vegetation recovers post-disturbance (including, but not limited to, fire) at a fine scale has been the subject of much research (Robinson et al. 2022; Rydgren et al. 1998; Samiappan et al. 2019). While drones are increasingly used for this process, the applications so far have not utilized the ability to digitally remove the overstory for understory classification. Previous work has been done to isolate overstory vs. understory in orthomosaic images derived from drone imagery (Herzog et al. 2022; Kolarik et al. 2019; Li et al. 2020) but this removal of tall vegetation for a classification of understory normally occluded, is a novel approach.

Objectives

To address the issue of isolating understory fire effects from overstory fire severity, we had three primary objectives in this methods paper:

- To generate multispectral photogrammetric point clouds from drone imagery for pre- and post-fire forest plots to quantify fire effects at different canopy height strata.
- Within the pre- and post-fire plots, to digitally remove all vegetation over 2 m to create classified orthoimages of understory-only vegetation.
- To compare our derived understory-only fire severity metric to satellite indices of the same area.

In forests with a relatively open overstory, this methodology facilitates the differentiation of understory fire effects from overstory fire effects, enables the monitoring of vegetation changes due to disturbance or regrowth with centimeter-level precision, and offers a tool to quantify the potential underestimation of fire effects as observed through aerial or satellite imagery.

Methods

Site

The study site was in SC, USA, on the US Army base Fort Jackson (Fig. 2). Fort Jackson occupies 20,767 hectares, with the dominant forest type consisting of fire adapted longleaf pine (*Pinus palustris* Mill.) with an understory dominated by sparkleberry (*Vaccinium arboreum* Marshall.). Longleaf pine forests have relatively open canopies, allowing aerial images to capture much of the ground. Fort Jackson uses repeated prescribed burning (Landers et al. 1990) across its pine forests to “manage fire safely and effectively to achieve desired ecological conditions while protecting assets and air quality and facilitating the military mission” (Cohen et al. 2014). The vegetation was typical of frequently-burned forest conditions in the Sand Hills region of the Carolinas with an open structure of longleaf pine, open midstory, sparse shrub layer with clumps of sparkleberry, and leaf litter primarily of longleaf pine needles (Porcher and Rayner 2001; Swezey et al. 2016).

Drone imagery was collected pre- and post-fire in seven replicate plots located in similar stands (Table 1). Each plot was approximately 0.2 ha and was selected for having an understory with a preponderance of sparkleberry. The size and locations of plots were partially dictated by existing roads that were used as fire breaks and to provide easy access, as well as the need to meet other research objectives associated with the burns; namely, to measure pyrolysis gas emissions from the sparkleberry shrubs (Weise et al. 2025). The plots had a naming convention to match additional studies associated with these burns (Banach et al. 2021; Herzog et al. 2022; Hudak et al. 2020; Scharko et al. 2019; Weise et al. 2024). Two of the plots were used as unburned controls (plots 2 and 3) and were flown twice, before and after the other plots were burned (plots 1, 5, 6, 24 A, and 24B).

dDAP point clouds

For the dDAP data, a DJI Mavic Pro drone (DJI 2016)[1] with a stock 12-megapixel RGB camera with a resolution of 3 cm/px at 100 m was used. A Parrot Sequoia multispectral camera (Parrot 2016) was alternatively attached to the drone such that images also were captured in four spectral bands: Green (GRE):530–570 nm, Red (RED):640–680 nm, Red Edge (REG):730–740 nm, and NIR (NIR):770–810 nm. The resolution of the parrot Sequoia images was 9 cm/px at 100 m. For image acquisitions, transects were flown over the plots at both 60 m and 120 m. Images were collected with a minimum of 80% front and side overlaps.

Image processing was performed using the photogrammetric Agisoft program, Metashape (Agisoft 2014). Photogrammetric point clouds were generated using all bands from the parrot sequoia. Radiometric calibration of the images was performed during processing using the data recorded from the camera’s sunlight sensor, as well as using a calibrated reflectance panel. Photogrammetric point clouds were also created using the RGB images from the Mavic Pro stock camera. Three-dimensional photogrammetric point clouds were created from both multispectral and RGB imagery for all plots, both before and after the fires (28 total point clouds). Each point in the resultant multispectral point clouds had the 4 sequoia spectral values associated with it. All points generated

[1] The use of trade or firm names in this publication is for reader information and does not imply endorsement by the U.S. Department of Agriculture of any product or service.

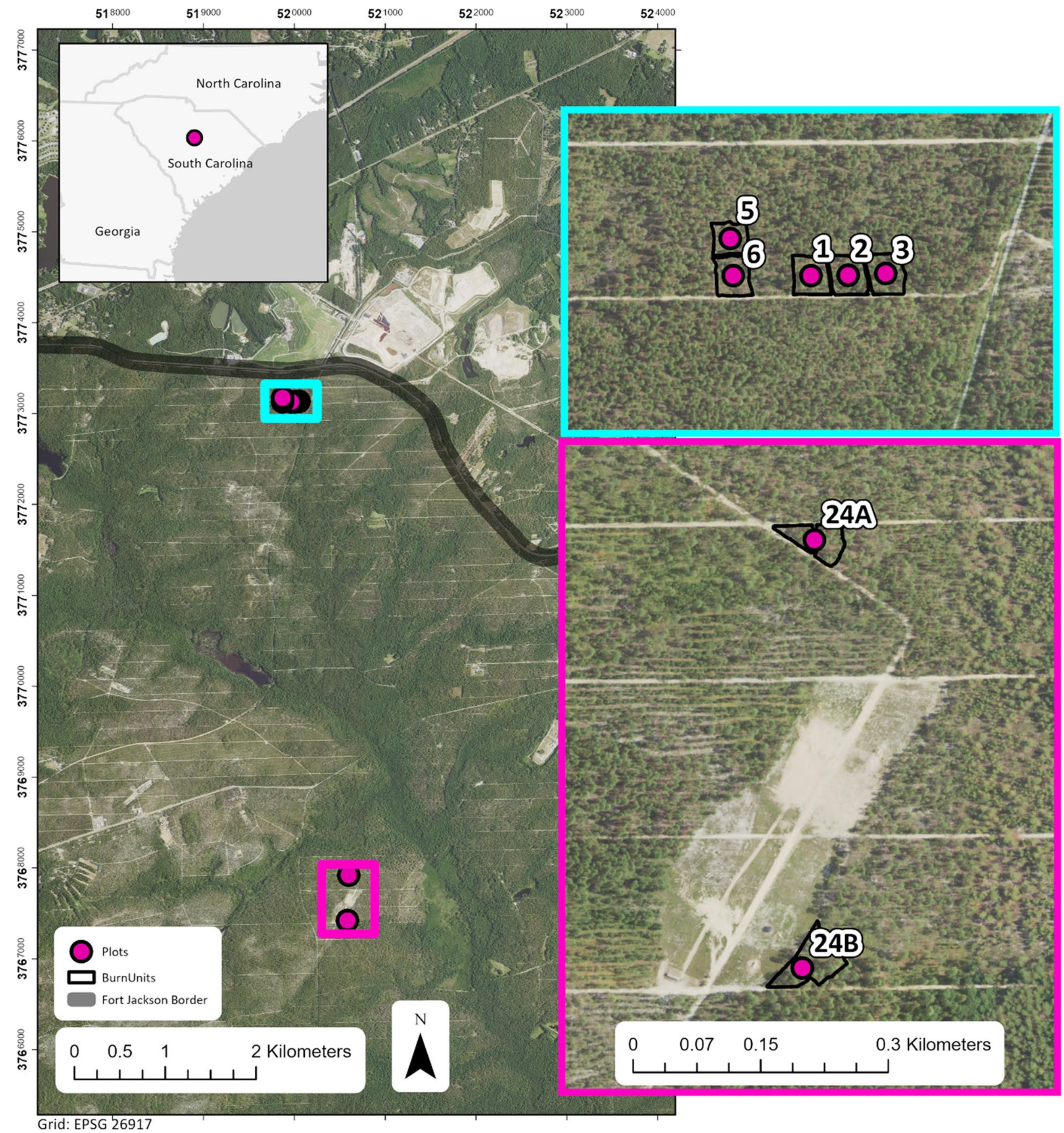

Fig. 2 Location of replicate plots within Fort Jackson, near Columbia, SC, USA. 2019 NAIP imagery basemap to provide context of vegetation cover. The east–west lines visible in the imagery are from plowed firebreaks the fort maintains

were used, as employing thresholds of minimum look angles for point generation and confidence intervals excluded a high percentage of valid vegetation points. Quality control was conducted visually to remove errant points and low-quality image inputs.

Using multispectral point clouds, the open-source program CloudCompare (CloudCompare 2019) was used to calculate the NDVI value for each point, such that normalized difference vegetation index (NDVI) point clouds could be generated (Fig. 3). Both pre- and post-burn NDVI point clouds were created for each of the seven plots (including the two unburned plots). In total, there were 14 NDVI point clouds created.

Table 1 Plot number, size, and time/date of each drone flight. Preexisting roads were partially used as fire breaks, so plot sizes varied. Flight times were generalized as flights averaged between 10 and 20 min. The times given are for RGB image collection, additional flights were required to collect multispectral imagery for some plots, and time was not recorded. Plots 2 and 3 were unburned

Plot #	*Size (ha)*	*Pre-burn flight time*	*Burn date*	*Post-burn flight time*
24B	0.31	10:00 2018–04–30	2018–05-01	11:00 2018–05-02
24 A	0.22	12:00 2018–04–30	2018–05-02	16:00 2018–05-02
5	0.15	14:00 2018–04–30	2018–05-03	14:00 2018–05-03
6	0.19	14:00 2018–04–30	2018–05-03	14:00 2018–05-03
1	0.18	15:00 2018–04–30	2018–05-03	13:00 2018–05-04
2	0.19	15:00 2018–04–30	Not burned	13:00 2018–05-04
3	0.2	15:00 2018–04–30	Not burned	13:00 2018–05-04

Each plot had four dDAP point clouds: pre-fire multispectral, post-fire multispectral, pre-fire RGB, and post-fire RGB. The pre-fire RGB dDAP point clouds were georectified using 2017 airborne lidar (ALS) of Fort Jackson to perform fine-scale point-cloud matching. Using aerial lidar and tree crown matching to georeference photogrammetric point clouds or terrestrial lidar point clouds is a method commonly used in place of surveying in ground control points (Batchelor et al. 2023; Hauglin et al. 2014). For each plot, the post-fire RGB, pre-fire multispectral, and post-fire multispectral were then co-registered with the geolocated pre-fire RGB point clouds. Root mean square error (RMSE) values for co-registered dDAP point clouds averaged between 5 and 10 cm. All subsequently derived rasters had this same co-registration error. This ensured a direct comparison between multiple datasets without compounding location errors. A 1-m digital terrain model derived from ALS was used to "normalize" the dDAP point clouds. This normalization subtracts all ground elevation values from the dDAP point cloud values, creating a "flat" scene in which the hill slope was removed. However, minimum normalization was required as all plots were relatively flat to begin with. All photogrammetric point clouds were then binned into 2-m height strata (Fig. 4).

Point cloud statistical analysis

Using the height strata, the pre- and post-fire NDVI point clouds were compared at each site. Two sample z-tests were performed to determine if there was a change in the mean NDVI values of points within each height stratum after the fire. In addition to a simple test of difference of means between groups of large sample sizes (typically > 10,000 in this case study), Cohen's d (Ben-Shachar et al. 2020; Cohen 1988) was used to assess the effect size of

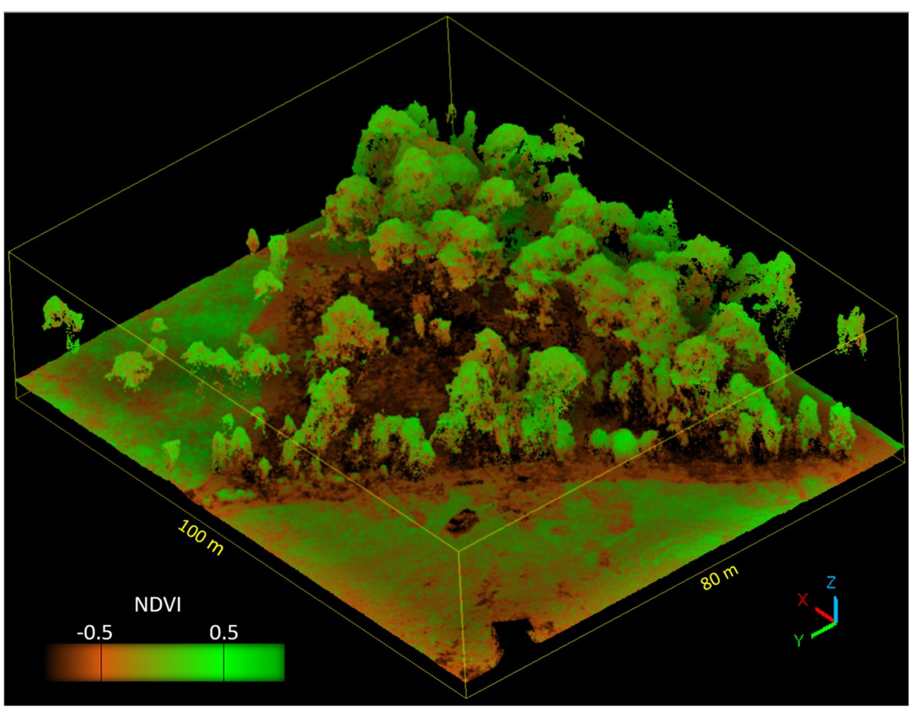

Fig. 3 NDVI point cloud generated from the multispectral photogrammetric point cloud of post-burn plot 24B and the surrounding area. Y is north, X is east

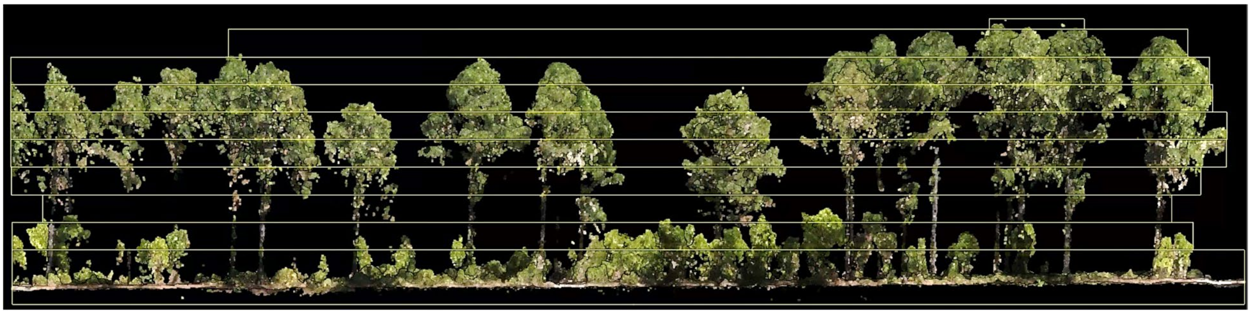

Fig. 4 Two-meter height strata highlighted in one of the height normalized RGB photogrammetric point clouds

the burns on the NDVI values of the points within each height stratum for the aggregated burned and unburned plots. Cohen's d is a method of determining the relative effect size of a treatment between two groups. With large data sets, small differences can become statistically significant, and Cohen's d is one method to contextualize difference by providing a standardized measure of effect size beyond simply reporting a difference in mean value between two groups. Cohen's d is a measure of the number of standard deviations between the two means of the compared datasets. Thresholds of effect size were set as follows: $d < 0.1$, very small; $0.1 \leq d \leq 0.5$, small; $0.5 < d \leq 0.8$, moderate; $0.8 < d \leq 1$, large; and $d > 1$, very large. The ordinal values from small to large were subjective, and the suggested thresholds (Cohen 1988) were used with the addition of the "very large" class to indicate plots in our study that had the largest effect size from fire. Point density violin plots of pre- and post-fire NDVI values were created from the values of the point clouds to visualize the change in the distribution of the values at strata of different heights.

Multispectral orthoimage processing

CloudCompare was used to convert the point clouds into raster orthoimages for both multispectral photogrammetric point clouds and RGB photogrammetric point clouds. From the multispectral point clouds, 20 cm resolution orthoimages were made from all points (the nadir view of the plots) and points 2 m and below (Fig. 5). Points above 2 m were used to create a third orthoimage raster denoting canopy cover only. The figures of all color-infrared orthoimages at all plots are included in the supplemental material. All three sets of multispectral photogrammetric point clouds (understory-only, nadir, and overstory-only) were used to create NDVI rasters of the pre- and post-burn plots, as well as dNDVI rasters.

Multispectral orthoimage analysis

Using the co-registered, 20 cm resolution, pre- and post-fire multispectral images, scatter plots of spatially matched raster cell NDVI values pre- and post-fire were created to visualize the shift in NDVI values. There were three sets of scatter plots: NDVI values for the matched cells in the understory-only orthoimages (e.g., Fig. 5A and C), NDVI values for matched cells in nadir orthoimages (e.g., Fig. 5B and D), and NDVI values for canopy-only matched cells. Assuming normality and standard normal deviates (z), paired z-tests were performed to determine if there was a significant difference between the pre- and post-fire NDVI values of the matched pixels (Zar 1974) in addition to using Cohen's d to quantify effect size. Cohen's d was performed on paired pixel data to assess the effect size of the fire on NDVI values. The same effect size thresholds were used as with the dDAP point cloud comparisons ("Point cloud statistical analysis" section). Density probability plots were created for all comparisons to illustrate the change in the distribution of NDVI values when comparing understory-only, nadir, and overstory-only imagery.

RGB orthoimage processing

Using CloudCompare, 5 cm resolution image rasters were produced from the RGB point clouds using only the points 2 m and below. Images of the RGB orthoimages for all plots are included in the supplemental material. The RGB values of each pixel were determined using the values of the point highest in elevation within each raster cell area. Owing to the complexity of the tree structures, 5 cm resolution images had too many gaps to effectively model the tree canopy extent. The 20 cm resolution rasters of all points greater than 2 m in height from the multispectral photogrammetric point clouds were used to determine the location and size of the canopy cover. The percentage of ground cover visible from a nadir view at each plot was calculated.

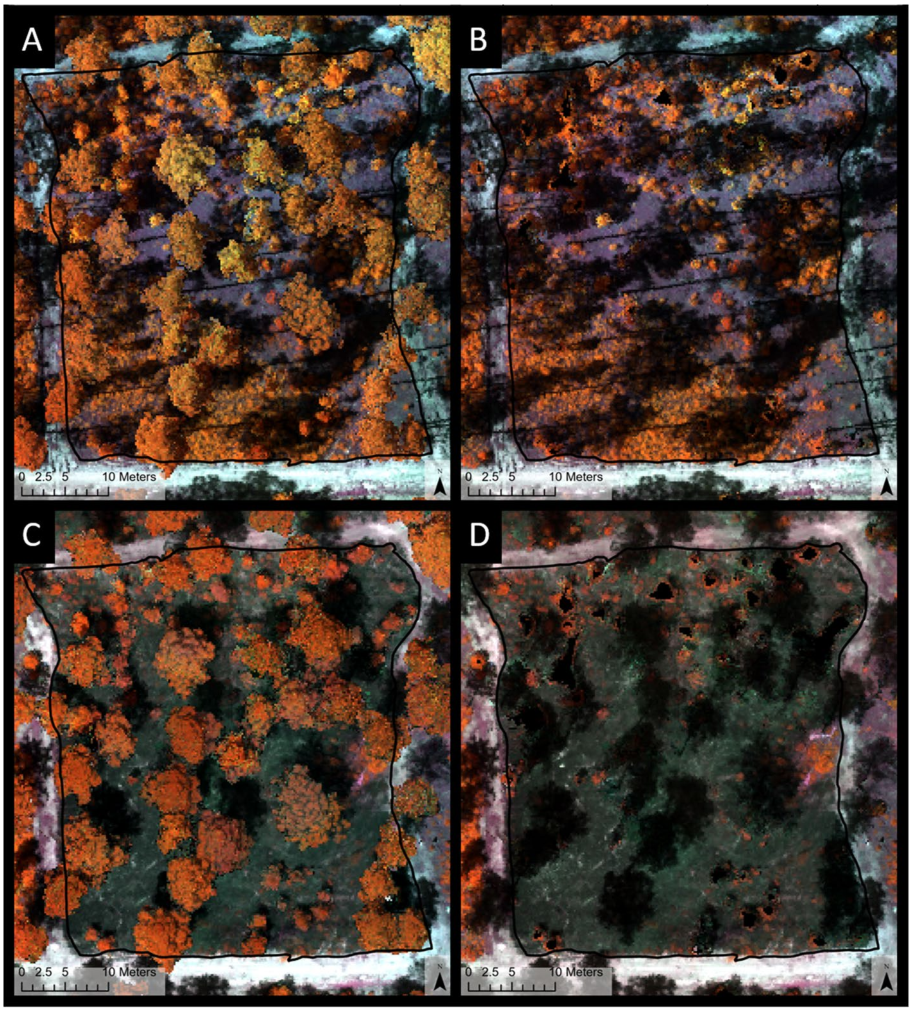

Fig. 5 Plot 6 as an example of a 20 cm resolution color infrared orthoimage (NIR, R, G) produced from a multispectral photogrammetric point cloud. **A** Pre-burn nadir, **B** pre-burn understory only, **C** post-burn nadir, **D** post-burn understory only. Multispectral and RGB orthoimages rendered from the point clouds for all plots are included in the supplemental material

Both the 20 cm resolution multispectral orthoimages and the 5 cm resolution RGB orthoimages were created through a process of rasterizing the photogrammetric point clouds. The difference in resolution between the two images sets was reflective of the resolution of the different cameras collecting the initial imagery. Conceptually, the cells of the multispectral raster represent a 20 × 20 cm column within the point cloud. We used the spectral values of points at the highest elevation within each column to generate nadir and overstory-only rasters. This is analogous to taking a photograph from a drone. Similarly, for the understory orthoimages, after removing all points above 2 m, we used the spectral values for the points closest to 2 m to generate the orthoimages. Other options could have been spectral values for the lowest elevation points, the mean, min, or max values for points, or any other statistical value derived from the points. Using the points closest to 2 m is most analogous to taking a nadir photo with all vegetation above 2 m removed, but using the lowest elevation points may provide a more accurate representation of ground conditions. We opted for the 2 m point values to include ground vegetation and produce NDVI values that included vegetation in the pre-burn images and to account for the scorching or consumption of that vegetation in the post-burn images.

RGB orthoimage analysis

RGB understory orthoimages were used to create pre-burn ground-cover classification maps with the following classes: bare ground, leaf litter, live vegetation, and woody debris. Post-burn classification maps were also produced with the same classes and additional classes of black char (areas of incomplete combustion) and white ash (areas of complete combustion). Object-based supervised classification (support vector machine) was used to classify each image.

Accuracy assessment was performed using a reference point density of 500 points per hectare. Points were placed in the classified images using a stratified random placement strategy. The reference was determined by viewing each point within the understory orthoimage independently without referring to the classification. Each point was assigned to a class of either Black Char, White Ash, Bare Ground, Leaf Litter, Woody Debris, or Ground Vegetation. A confusion matrix (Congalton and Green 2009) was produced to assess the accuracy rates of each class per plot as well as all plots combined.

Using height values from a vegetation height model created from the 0–2 m RGB photogrammetric point clouds (Fig. 6), live vegetation was further sub-divided into 2 classes of herbaceous vegetation (0–0.5 m) and shrub vegetation (taller than 0.5 m).

Multispectral dDAP dNDVI Comparison to Satellite dNDVI

With understory, overstory, and nadir dNDVI rasters (20 cm resolution) produced using multispectral dDAP data, comparison with satellite-derived dNDVI values was conducted. The pre- and post-burn satellite imagery from both Sentinel 2 (10 m resolution) and Landsat 8 (30 m resolution) sensors was acquired, and the dNDVI values were calculated (Table 2). Satellite dNDVI values for the unburned and burned plots were compared with the dNDVI values for the burned and unburned plots from understory-only and nadir dDAP NDVI images. The effect size was measured using Cohen's *d* test.

Table 2 Dates of the Sentinel and Landsat imagery used to derive NDVI values. The image dates used were based on data availability and lack of cloud cover

Pre-burn Sentinel date	Post-burn Sentinel date	Pre-burn Landsat date	Post-burn Landsat date
2018–04–29	2018–05–09	2018–04–14	2018–05–12

Results

dDAP point clouds

Violin plots of the distribution of NDVI values are presented in Fig. 7 for aggregated burned and unburned plots. Height strata comparisons were performed for all 2 m strata up to 18 m. Treetop vegetation in the plots was either sparse or non-existent above 18 m. The samples were the entirety of points within the generated multispectral photogrammetric point clouds at each height bin, so the sample sizes were very large. Each point represents a sample from within a height bin in either a plot that burned or did not burn. By including all points (the entire population), the standard deviation of samples is captured. This is important to derive a magnitude of

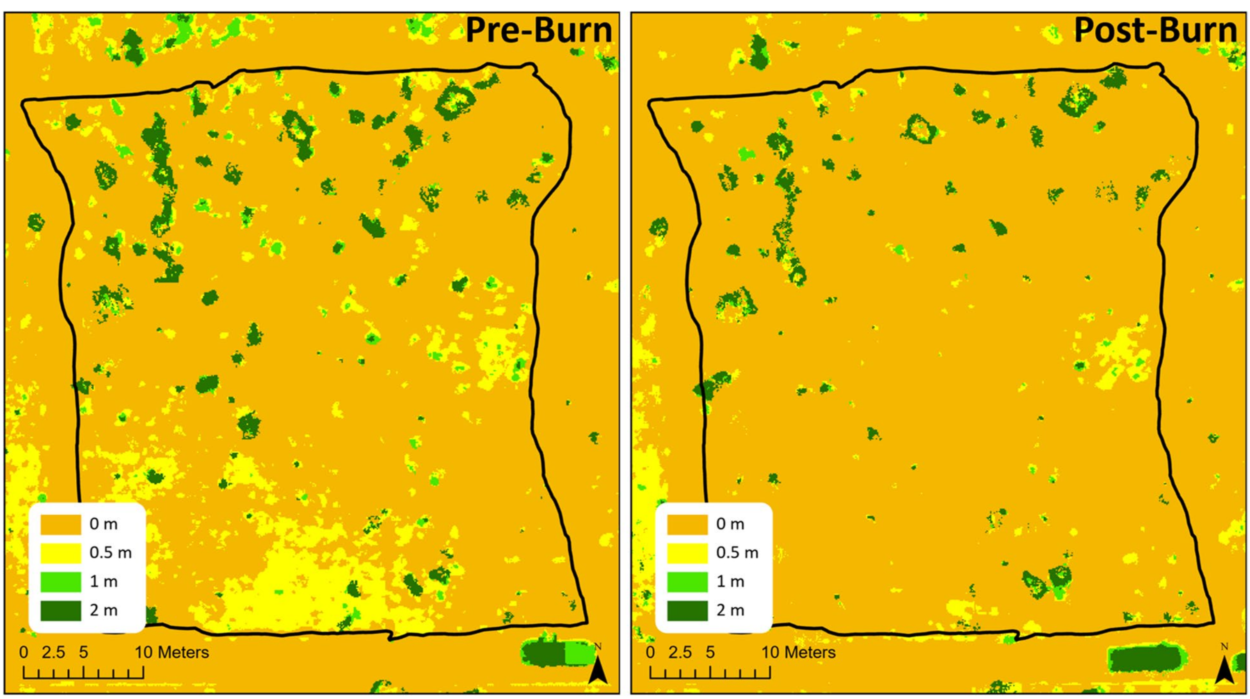

Fig. 6 Vegetation height models excluding all vegetation above 2 m for Plot 6. This is height above ground for understory vegetation allowing for the differentiation of herbaceous ground cover and shrubs taller than 0.5 m

Fig. 7 Pre- and post-burn NDVI value violin plots for burned (top) and unburned plots (bottom). The large sample sizes are all NDVI point cloud points within the respective height bins. The green side of the violins is the distribution of NDVI values pre-fire, with the brown side indicating the NDVI values post-fire. The numbers at the top of each violin are Cohen's *d* values, which quantify the effect size of the fire on NDVI values. Asterisks indicate: ****, very large effect; ***, large effect; **, medium effect; *, small effect; no asterisk, very small effect. The violins on the left represent the ground level, increasing in height to the right, up to 18 m. The median is indicated by the centerline in the box with one quantile above and below contained within the range of the rectangle

change between treatments (pre-burn/post-burn) that is quantified by using the Cohen's d value. All z-tests indicated a significant change in the mean NDVI value for all pre- vs post-fire comparisons at all height strata (p-value <0.001). Cohen's d values indicated either a small or very small effect size on the pre- and post-fire collected imagery in the unburned plots that were not burned, medium or small effect size in the burned plots above 10 m, and a very large effect size in burned plots below 6 m (Fig. 7).

Multispectral orthoimage

All z-tests comparing the burned plots to the unburned plots indicated a significant change in the mean NDVI value ($p < 0.001$). All z-tests comparing pre-fire to post-fire plot NDVI values indicated a significant change in the mean (p-value <0.001). The samples were the individual pixels within the orthoimages for the probability density plots and the matched pre- and post-fire pixels for the scatter plots. The sample sizes were between 52,000 and 241,000 pixels (Fig. 8).

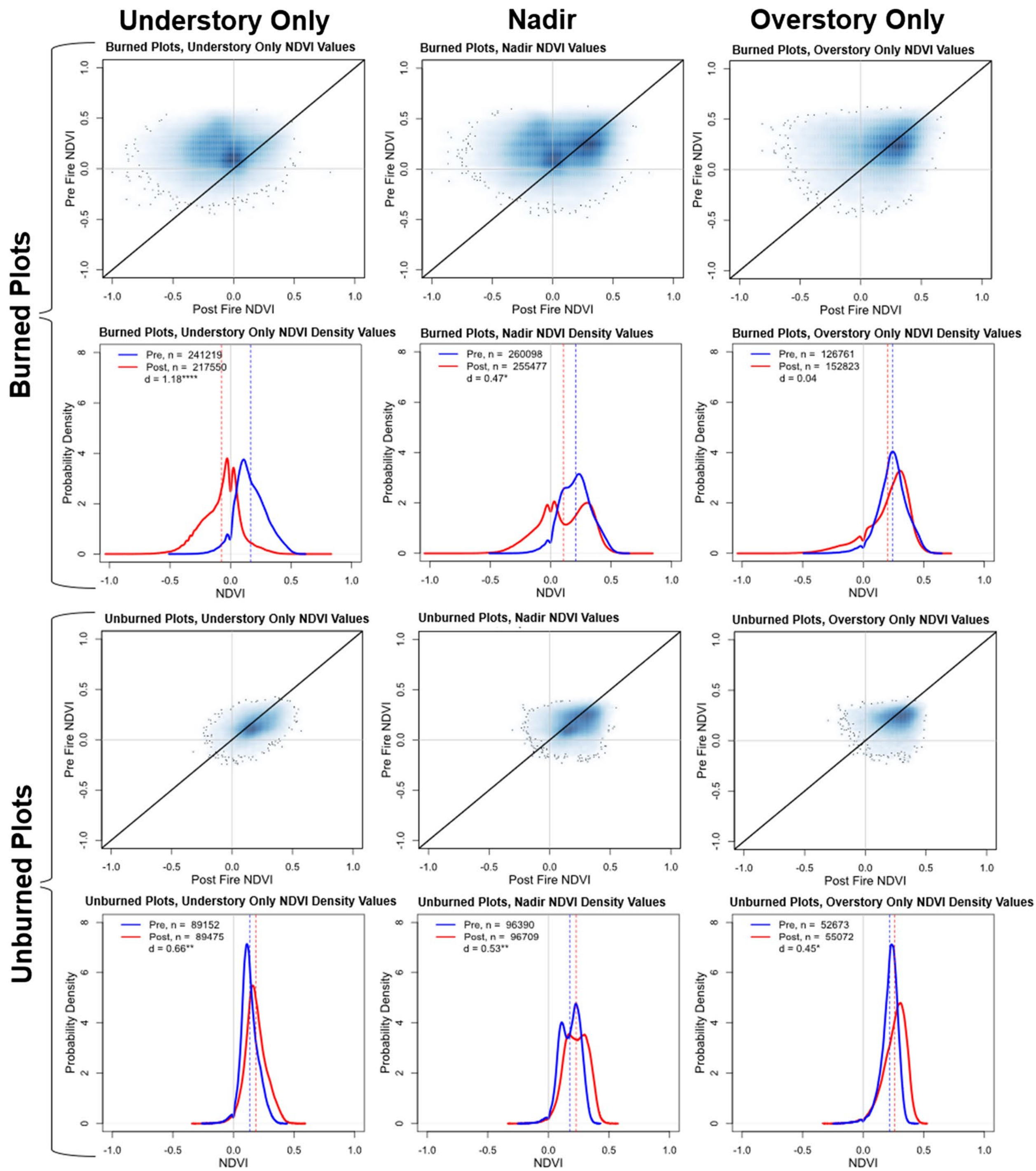

Fig. 8 Scatter and density plots comparing all burned plots (1, 5, 6, 24 A, and 24B) pre- and post-fire with unburned plots (2 and 3). Scatter plots are matched pixels before and after the burn. The black one-to-one line indicates where points should cluster if no change has taken place. If points are spread into the upper-left quadrant of the scatter plot, there is a decrease in the NDVI values post-fire. The density plots indicate the probability that a random pixel will have the indicated value. Dotted lines indicate mean values. The number of pixels used to generate the density plot is denoted as n. Cohen's *d* values quantifying the effect size of the fire on orthoimage NDVI values is given as d with asterisks indicating effect size. **** very large effect, *** large effect, ** medium effect, * small effect, no asterisk: very small effect

The scatter and density plots for the aggregated burned and unburned plots are presented in Fig. 8. Cohen's *d* values for the effect size indicated a small or medium effect for the pre- and post-fire imagery in the unburned plots as well as the nadir and overstory-only imagery in the burned plots. The understory-only orthoimages from the burned plots had a very high effect size between the pre- and post-fire imagery (Fig. 8).

Unlike the RGB orthoimages, the understory multispectral orthoimages did not achieve complete coverage. In areas with larger continuous tree canopy coverage, such as the east side of plot 24 A (see Appendix 1), there were gaps in understory coverage. These gaps increased with the extent of continuous canopy coverage. Smaller areas of continuous canopy, typically from individual trees, did not occlude the ground. However, larger areas of continuous canopy, usually formed by clumps of multiple trees, did cause ground occlusion. The percentage of each plot captured in the understory-only multispectral orthoimages, and the percentage of the area occluded by trees for each plot, are presented in Table 3. There was variation in the upper canopy region as measured from pre- and post-fire imagery. The values given as Overstory % are the average between the two.

Table 3 Percentage of the ground that could be modeled using multispectral orthoimages for each plot, both pre-burn (Pre %) and post-burn (Post %). The percentage of the ground occluded from nadir by vegetation over 2 m (i.e., trees) is given as Overstory %

Plot	*Pre %*	*Post %*	*Overstory %*
1	86	81	67
2	94	93	55
3	90	92	55
5	99	93	44
6	98	91	43
24 A	87	70	70
24B	95	86	47

RGB orthoimage classification

Of the 1.44 hectare total area of all plots, 0.88 hectares had occluding vegetation above 2 m (61% ground occlusion). Ground cover was classified with an overall accuracy of 87% (Fig. 9, Table 4., and Appendix 2).

Multispectral dDAP dNDVI comparison to satellite dNDVI

The number of samples from each image source reflects the resolution of the images. The number of samples for each imagery source and the Cohen's *d* value for the effect size are presented in the boxplot in Fig. 10. The difference

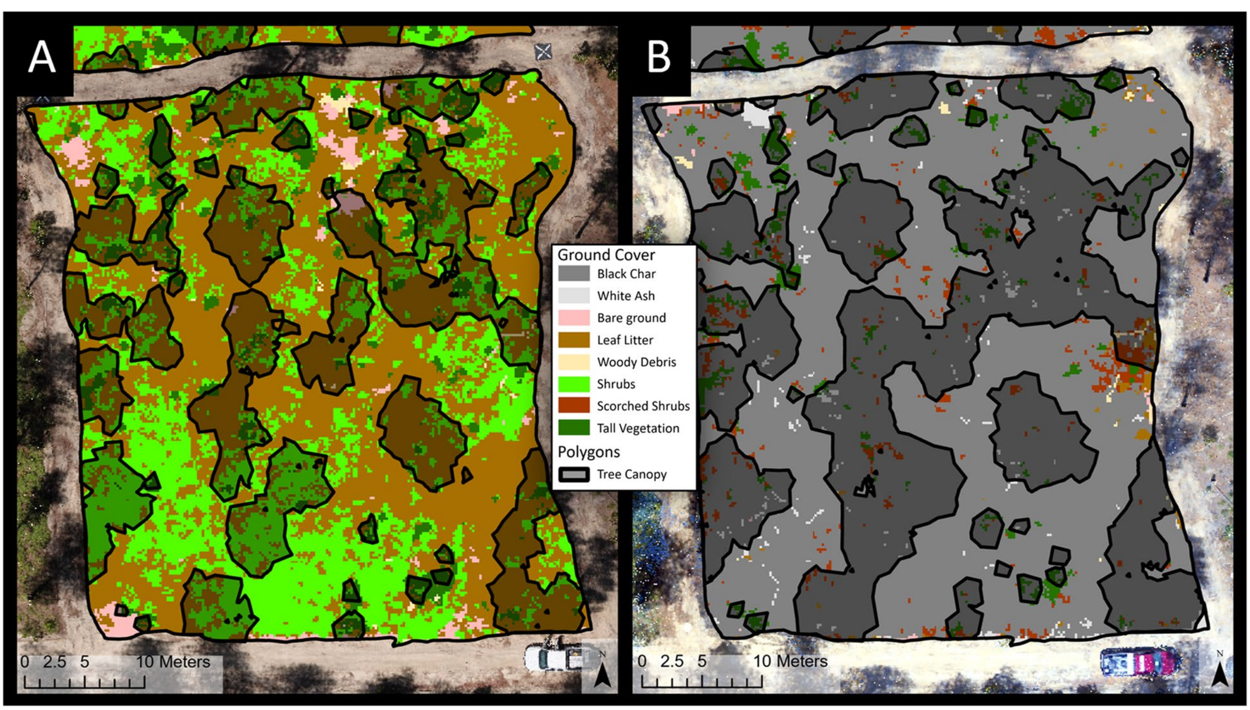

Fig. 9 Classification of Plot 6: pre-burn (**A**) and post-burn (**B**). The shaded polygons with black outlines are the area occupied by live tree crowns that were digitally removed to be able to do a complete understory classification. Classified images for all plots are provided in the supplemental material as well as the RGB orthoimages that show the live crown

Table 4 Confusion matrix for all plots pre-burn (top) and post-burn (bottom). The post-burn classification had two additional classes of black char and white ash that were not present in the pre-fire imagery. The total accuracy combining the pre- and post-fire imagery was 87% (kappa = 0.84)

Reference									
	Pre-Burn	Bare Ground	Leaf Litter	Woody Debris	Understory Vegetation	Total	Users Accuracy		
Classification	Bare Ground	**54**	2	4	1	61	0.89		
	Leaf Litter	2	**143**	0	18	163	0.88		
	Woody Debris	4	1	**12**	1	18	0.67		
	Ground Vegetation	0	11	2	**129**	142	0.91		
	Total	60	157	18	149	384			
	Producers Accuracy	0.9	0.91	0.67	0.87		Overall Accuracy 0.88		
	Post-Burn	Black Char	White Ash	Bare Ground	Leaf Litter	Woody Debris	Understory Vegetation	Total	Users Accuracy
Classification	Black Char	**166**	1	1	0	0	12	180	0.92
	White Ash	2	**29**	8	0	0	1	40	0.73
	Bare Ground	0	1	**45**	0	2	2	50	0.9
	Leaf Litter	0	0	3	**49**	0	5	57	0.86
	Woody Debris	0	1	15	2	**12**	0	30	0.4
	Ground Vegetation	2	0	0	0	0	**65**	67	0.97
	Total	170	32	72	51	14	85	424	
	Producers Accuracy	0.98	0.91	0.63	0.96	0.86	0.76		Overall Accuracy 0.86

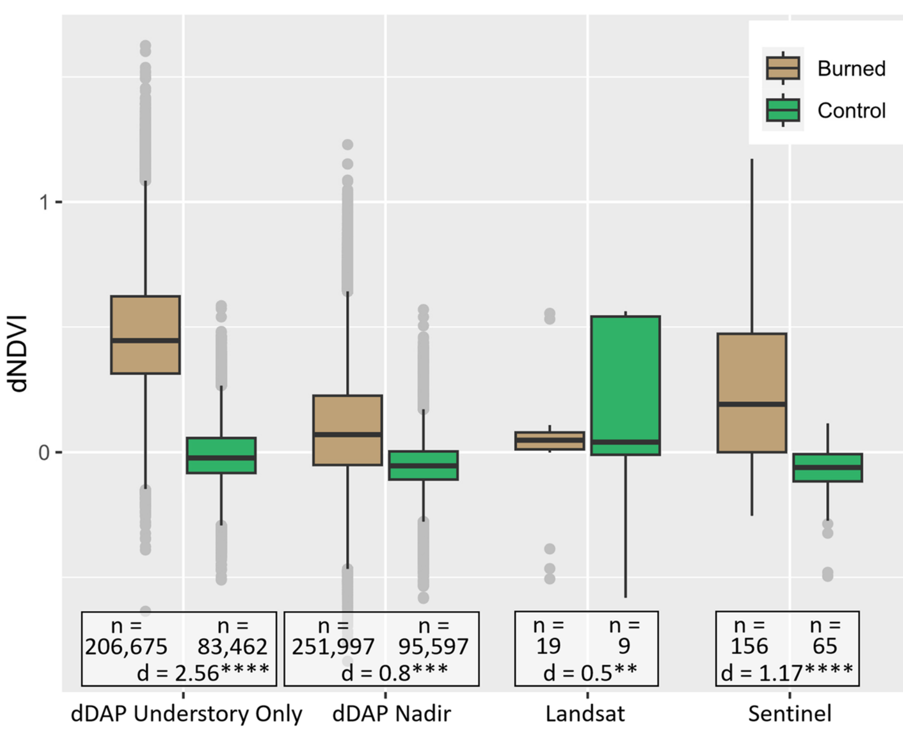

Fig. 10 Distribution of the dNDVI values for the four comparison groups

in the n value for the dDAP understory compared to the dDAP nadir is due to some gaps present in the multispectral understory only orthoimages as discussed in the "Multispectral orthoimage" section (Table 3). The fire had a medium and small effect on the measured dNDVI values of the dDAP nadir and Landsat imagery, respectively. There was a very large effect on the recorded dNDVI values of dDAP Understory and Sentinel imagery. Although both effects were categorized as very large, the effect size was more than double when quantifying dNDVI values using dDAP understory imagery.

Discussion

dDAP point clouds

The first objective of this study was to generate multispectral photogrammetric point clouds to quantify fire effects at differing height strata. Within our generated point clouds, our measured effect size was very large for strata lower than 6 m in our burned plots and was small in our unburned plots, indicating that our methodology quantifies the difference in fire effect size between burned and unburned plots. Within the burned plots, the effect size of the burn was larger in the height strata below 6 m compared to the height strata above, indicating that we were able to differentiate fire effects at different heights. The effect size was larger in the 16–18 m stratum (0.73) in the burned plots than in the strata between 8 and 16 m. There are several potential reasons for this difference. The upper strata represented the bulk of the tree canopy, and there could have been crown scorching from lower flames. The strata between 8 and 16 m were largely comprised of tree boles that would be less likely to have a change in NDVI values. The values are for the aggregated point clouds of all sites, but points associated with individual trees could be segmented out, and potentially a measurement of scorch per tree could be derived.

The first-order fire effects on live vegetation, including scorching and combustion, and the subsequent changes in NDVI are well established (White et al. 1996). The gradual recovery and eventual stabilization of NDVI values in satellite imagery have been used to document post-fire recovery (João et al. 2018; Kennedy et al. 2010; Lacouture et al. 2020). We propose that this novel photogrammetric point cloud method offers a way to quantify changes in NDVI in three dimensions, highlighting areas of change within the vertical structure, similar to change detection with satellite imagery. It allows for the documentation of the initial magnitude of change in NDVI values at any point within the vertical structure and provides a method to document recovery over time at different height strata. Our results demonstrating the ability to quantify the magnitude of change in NDVI between pre- and post-fire photogrammetric point clouds are similar to other post-fire only photogrammetric point cloud analysis comparing NDVI values of green vs scorched conifer needles (Moran et al. 2022). Defoliation and crown scorch have been shown to lead to reduced growth rates, decreased root nutrient concentrations, and mortality in longleaf pine trees (Sayer et al. 2020; Sword and Haywood 1995; Weise et al. 2016). Utilizing multispectral photogrammetric point clouds for three-dimensional quantification of crown scorch at such fine scale could enhance estimates of both immediate and delayed fire effects in such systems.

Orthoimages

While drones are seeing increased use to capture multispectral imagery to quantify disturbance events such as fire (Carvajal-Ramírez et al. 2019; Iheaturu et al. 2024; Larrinaga and Brotons 2019; Shin et al. 2019), our process of digitally removing points above 2 m from the photogrammetric point cloud and then creating rasters from the lower points, is a new and novel process. Detection of change, either by fire consumption or vegetation regeneration, at a centimeter level of accuracy is possible via drone (Hüttnerová et al. 2024; Mestre-Runge et al. 2023). Establishing semi-permanent ground control points to co-register image acquisitions at different times would allow for tracking of first order fire effects as well as subsequent regeneration.

In this study, we classified fine-scale understory land cover with high overall accuracy, though accuracy levels varied by class. Woody debris had relatively low user accuracy (67% pre-burn, 40% post-burn) due to the spectral similarity between light-colored downed wood and sandy soil. In contrast, other classes, such as black char, showed extremely high accuracy levels (92% user accuracy and 98% producer accuracy) because of their distinctive appearance. In our classification, we included shadowed areas, as it was still possible to visually identify the classes for the accuracy assessment, even when they were in shadow. To further aid in separation of low vegetation (below 0.5 m) and tall vegetation (up to 2 m), a digital surface model was created from the photogrammetric point cloud. Similar approaches combining photogrammetric DSMs with spectral information from drone imagery have similarly shown an increase in classification accuracy when compared to using only spectral information (Cunliffe et al. 2016; Prošek and Šímová, 2019).

Our approach could aid in fine-scale mapping of vegetation cover changes in areas that would normally be occluded from overhead imagery and where ground access is not possible (due to unexploded ordinance or other hazards). This could be especially important for identifying small fire refugia pockets which are important for the initial survival of species as well as their ability to propagate post-fire (Blomdahl et al. 2019; Marsh et al. 2022).

Comparison to satellite dNDVI

Our initial findings on how dDAP can quantify understory and overstory fire effects compared to the 2D imaging capabilities of satellite imagery reinforces previous research conclusions that satellite imagery burn indices do not always accurately capture fire effects compared to field observations (Miller et al. 2023; Parks et al. 2019; Saberi et al. 2022). With our plots being relatively small in relation to the pixel sizes of Landsat and Sentinel data, there would be considerable spectral mixing of unburned and burned forested areas. The nineteen 30 m Landsat pixels used to derive dNDVI values were sampling areas outside the burn perimeter, which likely contributed to the Landsat data only detecting a medium effect size, while the Sentinel data at 10 m resolution had 156 pixels within our burn parameters (Fig. 10). Even with a small fire, this methodology of using drone imagery to digitally remove overstory vegetation to derive dNDVI values for the understory only, measured a fire effect size more than double that of the Sentinel data. Thus, illustrating the tendency of satellite burn indices to underestimate the burn severity of surface fires.

Future research

The methods presented here demonstrate the utility of photogrammetric point clouds for fire effects assessments. One limitation of this study that should be addressed in future research is how camera resolution, flight patterns, and photogrammetry processing affect point cloud generation. These topics for generalized dDAP acquisition have been addressed in numerous previous studies (Iglhaut et al. 2019; Kameyama and Sugiura 2021; Koci et al. 2017; Westoby et al. 2012), but only in broader terms of the performance of structure-from-motion to produce reliable vegetation models. This study used a novel approach of orthoimage generation that would be more robust if a more complete 3D model of tree stems could be produced. The ability to produce more complete multispectral photogrammetric point clouds from drone imagery is likely to increase as both drone and camera technologies advance. With increased modeling performance and longer drone flights, repeating this research across larger post-fire areas could aid in the fine-scale mapping of revegetation and tracking post-fire upper canopy die off. Beyond drone imagery applications, creating multispectral photogrammetric point clouds and subsequent 3D spectral indices metrics from imagery acquired by crewed airplanes or satellites should be explored as both sources of imagery are already being used to generate 3D models from images (Alonzo et al. 2020; Yin et al. 2023). Having a quantified value for the area of understory vegetation consumed by fire can also improve models that use area consumed for emissions estimations (e.g., smoke emission modeling). Furthermore, it could be informative to test how well the three-dimensional characterization of fire effects from drone imagery compares to field assessments of fire severity.

Conclusion

Drones have become indispensable tools in ecological monitoring. The utility and application of drones will continue to expand as the technology develops. In this study we explored the possibility of generating full three-dimensional models of forests with multispectral imagery. Our methodology requires a relatively open overstory to allow for the capture of the ground and understory vegetation, but the ability to isolate understory vs overstory fire effects with spatial precision of a few centimeters will allow for fine scale quantification and monitoring of change post disturbance. Furthermore, this process of isolating understory-only dNDVI orthoimages with the removal of live upper canopy foliage will aid in a much more robust and fine-scale assessment of fire severity than is possible using nadir imagery alone.

Supplementary Information

The online version contains supplementary material available at https://doi.org/10.1186/s42408-025-00375-2.

Supplementary Material 1

Authors' contributions

Jonathan L. Batchelor: conceptualization, methodology, validation, formal analysis, software, investigation, data curation, writing—original draft, visualization. Andrew T. Hudak: conceptualization, writing—review and editing, project administration. Akira Kato: conceptualization, writing—review and editing. David R. Weise: writing—review and editing, funding acquisition, project administration. L. Monika Moskal: conceptualization, writing—review and editing, funding acquisition, project administration, supervision, resources.

Funding

This work was supported by the DOD/DOE/EPA Strategic Environmental Research and Development Program project RC-2640. USDA Forest Service annual research appropriations provided in-kind support from 2016–2022. This work was further funded by the Precision Forestry Cooperative at University of Washington.

Strategic Environmental Research and Development Program,RC-2640,David R. Weise,University of Washington Precision Forestry Cooperative

Data availability

Drone orthophotos and videos are available on the Wildland Fire Science Initiative data portal https://portal.wfsi-data.org/view/doi:https://doi.org/10.60594/W48G6B (Weise et al. 2025).

Declarations

Ethics approval and consent to participate
Not applicable.

Consent for publication
Not applicable.

Competing interests
The authors declare that they have no known competing financial interests or personal relationships that could have appeared to influence the work reported in this paper.

Author details
[1]School of Environmental and Forest Sciences, University of Washington, Seattle, WA 98195, USA. [2]USDA Forest Service, Rocky Mountain Research Station, Moscow, ID 83843, USA. [3]Chiba University Graduate School of Horticulture, Chiba, Japan. [4]USDA Forest Service, Pacific Southwest Research Station, Riverside, CA 92507, USA.

Received: 31 May 2024 Accepted: 26 April 2025
Published online: 23 June 2025

References
Agee, J.K., 1996. The influence of forest structure on fire behavior, in: Proceedings of the 17th Annual Forest Vegetation Management Conference. pp. 16–18.
Agisoft, 2014. Metashape 2020 [WWW Document]. URL https://www.agisoft.com/ (Accessed 10.5.23).
Alonzo, M., R. J. Dial, B. K. Schulz, H.-E. Andersen, E. Lewis-Clark, B. D. Cook, and D. C. Morton. 2020. Mapping tall shrub biomass in Alaska at landscape scale using structure-from-motion photogrammetry and lidar. *Remote Sensing of Environment* 245 : 111841. https://doi.org/10.1016/j.rse.2020.111841.
Amroussia, M., O. Viedma, H. Achour, and C. Abbes. 2023. Predicting Spatially Explicit Composite Burn Index (CBI) from Different Spectral Indices Derived from Sentinel 2A: A Case of Study in Tunisia. *Remote Sensing* 15:335. https://doi.org/10.3390/rs15020335.
Banach, C. A., A. M. Bradley, R. G. Tonkyn, O. N. Williams, J. Chong, D. R. Weise, T. L. Myers, and T. J. Johnson. 2021. Dynamic infrared gas analysis from longleaf pine fuel beds burned in a wind tunnel: Observation of phenol in pyrolysis and combustion phases. *Atmospheric Measurement Techniques* 14:2359–2376.
Batchelor, J. L., A. T. Hudak, P. Gould, and L. M. Moskal. 2023. Terrestrial and Airborne Lidar to Quantify Shrub Cover for Canada Lynx (Lynx canadensis) Habitat Using Machine Learning. *Remote Sensing* 15:4434. https://doi.org/10.3390/rs15184434.
Beaty, R. M., and A. H. Taylor. 2001. Spatial and temporal variation of fire regimes in a mixed conifer forest landscape, Southern Cascades, California, USA. *Journal of Biogeography* 28:955–966. https://doi.org/10.1046/j.1365-2699.2001.00591.x.
Ben-Shachar, M., Lüdecke, D., Makowski, D., 2020. effectsize: Estimation of Effect Size Indices and Standardized Parameters. JOSS 5, 2815. https://doi.org/10.21105/joss.02815
Bessie, W. C., and E. A. Johnson. 1995. The Relative Importance of Fuels and Weather on Fire Behavior in Subalpine Forests. *Ecology* 76:747–762. https://doi.org/10.2307/1939341.
Blomdahl, E. M., C. A. Kolden, A. J. H. Meddens, and J. A. Lutz. 2019. The importance of small fire refugia in the central Sierra Nevada, California, USA. *Forest Ecology and Management* 432:1041–1052. https://doi.org/10.1016/j.foreco.2018.10.038.
Cao, L., H. Liu, X. Fu, Z. Zhang, X. Shen, and H. Ruan. 2019. Comparison of UAV LiDAR and digital aerial photogrammetry point clouds for estimating forest structural attributes in subtropical planted forests. *Forests* 10:145.
Carvajal-Ramírez, F., J. R. Marques da Silva, F. Agüera-Vega, P. Martínez-Carricondo, J. Serrano, and F. J. Moral. 2019. Evaluation of Fire Severity Indices Based on Pre- and Post-Fire Multispectral Imagery Sensed from UAV. *Remote Sensing* 11:993. https://doi.org/10.3390/rs11090993.
Cary, A. 1932. Some Relations of Fire to Longleaf Pine. *Journal of Forestry* 30:594–601. https://doi.org/10.1093/jof/30.5.594.
CloudCompare [Computer Software]; Version 2.11; 2019. Available online: http://www.cloudcompare.org (accessed on 1 March 2021)., 2019. . (GPL software).
Cohen, J. (1988). Statistical Power Analysis for the Behavioral Sciences (2nd ed.). Routledge. https://doi.org/10.4324/9780203771587.
Cohen, S., J. Hall, and J. K. Hiers. 2014. *Fire Science Strategy: Resource Conservation and Climate Change, Strategic Environmental Research and Development Program*. USA: Resource Conservation and Climate Change Program Area. Washington D.C.
Colomina, I., and P. Molina. 2014. Unmanned aerial systems for photogrammetry and remote sensing: A review. *ISPRS Journal of Photogrammetry and Remote Sensing* 92:79–97. https://doi.org/10.1016/j.isprsjprs.2014.02.013.
Congalton, R. G., and K. Green. 2009. *Assessing the accuracy of remotely sensed data: Principles and practices*, 2nd ed. Boca Raton: CRC Press/Taylor & Francis.
Cunliffe, A. M., R. E. Brazier, and K. Anderson. 2016. Ultra-fine grain landscape-scale quantification of dryland vegetation structure with drone-acquired structure-from-motion photogrammetry. *Remote Sensing of Environment* 183:129–143. https://doi.org/10.1016/j.rse.2016.05.019.
DJI, 2016. Mavic Pro 2016 [WWW Document]. URL https://www.dji.com/mavic (Accessed 10.5.23).
Escuin, S., R. Navarro, and P. Fernández. 2008. Fire severity assessment by using NBR (Normalized Burn Ratio) and NDVI (Normalized Difference Vegetation Index) derived from LANDSAT TM/ETM images. *International Journal of Remote Sensing* 29:1053–1073. https://doi.org/10.1080/01431160701281072.
Fawcett, D., C. Panigada, G. Tagliabue, M. Boschetti, M. Celesti, A. Evdokimov, K. Biriukova, R. Colombo, F. Miglietta, and U. Rascher. 2020. Multi-scale evaluation of drone-based multispectral surface reflectance and vegetation indices in operational conditions. *Remote Sensing* 12:514.
Filippelli, S. K., M. A. Lefsky, and M. E. Rocca. 2019. Comparison and integration of lidar and photogrammetric point clouds for mapping pre-fire forest structure. *Remote Sensing of Environment* 224:154–166. https://doi.org/10.1016/j.rse.2019.01.029.
Hardin, P. J., and T. J. Hardin. 2010. Small-scale remotely piloted vehicles in environmental research. *Geography Compass* 4:1297–1311.
Hauglin, M., V. Lien, E. Næsset, and T. Gobakken. 2014. Geo-referencing forest field plots by co-registration of terrestrial and airborne laser scanning data. *International Journal of Remote Sensing* 35:3135–3149. https://doi.org/10.1080/01431161.2014.903440.
Herzog, M. M., A. T. Hudak, D. R. Weise, A. M. Bradley, R. G. Tonkyn, C. A. Banach, T. L. Myers, B. C. Bright, J. L. Batchelor, and A. Kato. 2022. Point cloud based mapping of understory shrub fuel distribution, estimation of fuel consumption and relationship to pyrolysis gas emissions on experimental prescribed burns. *Fire* 5:118.
Hoe, M. S., C. J. Dunn, and H. Temesgen. 2018. Multitemporal LiDAR improves estimates of fire severity in forested landscapes. *International Journal of Wildland Fire* 27:581–594.
Hoffrén, R., M. T. Lamelas, and J. de la Riva. 2023. UAV-derived photogrammetric point clouds and multispectral indices for fuel estimation in Mediterranean forests. *Remote Sensing Applications: Society and Environment* 31 : 100997. https://doi.org/10.1016/j.rsase.2023.100997.
Hudak, A. T., A. Kato, B. C. Bright, E. L. Loudermilk, C. Hawley, J. C. Restaino, R. D. Ottmar, G. A. Prata, C. Cabo, and S. J. Prichard. 2020. Towards spatially explicit quantification of pre-and postfire fuels and fuel consumption from traditional and point cloud measurements. *Forest Science* 66:428–442.
Hüttnerová, T., Muscarella, R., Surový, P., 2024. Drone microrelief analysis to predict the presence of naturally regenerated seedlings. Front. For. Glob. Change 6. https://doi.org/10.3389/ffgc.2023.1329675
Iglhaut, J., C. Cabo, S. Puliti, L. Piermattei, J. O'Connor, and J. Rosette. 2019. Structure from Motion Photogrammetry in Forestry: A Review. *Curr Forestry Rep* 5:155–168. https://doi.org/10.1007/s40725-019-00094-3.
Iheaturu, C. J., S. Hepner, J. L. Batchelor, G. A. Agonvonon, F. O. Akinyemi, V. R. Wingate, and C. Ifejika Speranza. 2024. Integrating UAV LiDAR and multispectral data to assess forest status and map disturbance severity in a West African forest patch. *Ecological Informatics* 84 : 102876. https://doi.org/10.1016/j.ecoinf.2024.102876.

João, T., G. João, M. Bruno, and H. João. 2018. Indicator-based assessment of post-fire recovery dynamics using satellite NDVI time-series. *Ecological Indicators* 89:199–212. https://doi.org/10.1016/j.ecolind.2018.02.008.

Kameyama, S., and K. Sugiura. 2021. Effects of differences in structure from motion software on image processing of unmanned aerial vehicle photography and estimation of crown area and tree height in forests. *Remote Sensing* 13:626.

Kane, V. R., J. A. Lutz, S. L. Roberts, D. F. Smith, R. J. McGaughey, N. A. Povak, and M. L. Brooks. 2013. Landscape-scale effects of fire severity on mixed-conifer and red fir forest structure in Yosemite National Park. *Forest Ecology and Management* 287:17–31.

Kato, A., L. M. Moskal, J. L. Batchelor, D. Thau, and A. T. Hudak. 2019. Relationships between Satellite-Based Spectral Burned Ratios and Terrestrial Laser Scanning. *Forests* 10:444. https://doi.org/10.3390/f10050444.

Keeley, J. E. 2009. Fire intensity, fire severity and burn severity: A brief review and suggested usage. *International Journal of Wildland Fire* 18:116–126.

Kennedy, R. E., Z. Yang, and W. B. Cohen. 2010. Detecting trends in forest disturbance and recovery using yearly Landsat time series: 1. LandTrendr — Temporal segmentation algorithms. *Remote Sensing of Environment* 114:2897–2910. https://doi.org/10.1016/j.rse.2010.07.008.

Key, C.H., Benson, N.C., 2006. Landscape Assessment (LA). In: Lutes, Duncan C.; Keane, Robert E.; Caratti, John F.; Key, Carl H.; Benson, Nathan C.; Sutherland, Steve; Gangi, Larry J. 2006. FIREMON: Fire effects monitoring and inventory system. Gen. Tech. Rep. RMRS-GTR-164-CD. Fort Collins, CO: U.S. Department of Agriculture, Forest Service, Rocky Mountain Research Station. p. LA-1–55 164.

Koci, J., B. Jarihani, J. X. Leon, R. C. Sidle, S. N. Wilkinson, and R. Bartley. 2017. Assessment of UAV and ground-based structure from motion with multi-view stereo photogrammetry in a gullied savanna catchment. *ISPRS International Journal of Geo-Information* 6:328.

Kolarik, N. E., G. Ellis, A. E. Gaughan, and F. R. Stevens. 2019. Describing seasonal differences in tree crown delineation using multispectral UAS data and structure from motion. *Remote Sensing Letters* 10:864–873. https://doi.org/10.1080/2150704X.2019.1629708.

Lacouture, D. L., E. N. Broadbent, and R. M. Crandall. 2020. Detecting Vegetation Recovery after Fire in A Fire-Frequented Habitat Using Normalized Difference Vegetation Index (NDVI). *Forests* 11:749. https://doi.org/10.3390/f11070749.

Landers, J.L., 1991. Disturbance influences on pine traits in the southeastern United States, in: Proceedings of the Tall Timbers Fire Ecology Conference. Tall Timbers Research Station Tallahassee, FL, USA, pp. 61–98.

Landers JL, Byrd NA, Komarek R (1990) A holistic approach to managing longleaf pine communities. In: Farrar Jr. RM (ed) Proceedings of the Symposium on the Management of Longleaf Pine. Gen. Tech. Rep. SO-75. USDA Forest Service, Southern Forest Experiment Station, New Orleans, LA, pp 135–167

Larrinaga, A. R., and L. Brotons. 2019. Greenness Indices from a Low-Cost UAV Imagery as Tools for Monitoring Post-Fire Forest Recovery. *Drones* 3:6. https://doi.org/10.3390/drones3010006.

Li, L., J. Chen, X. Mu, W. Li, G. Yan, D. Xie, and W. Zhang. 2020. Quantifying Understory and Overstory Vegetation Cover Using UAV-Based RGB Imagery in Forest Plantation. *Remote Sensing* 12:298. https://doi.org/10.3390/rs12020298.

Lydersen, J.M., Collins, B.M., Miller, J.D., Fry, D.L., Stephens, S.L., 2016. Relating Fire-Caused Change in Forest Structure to Remotely Sensed Estimates of Fire Severity. fire ecol 12, 99–116. https://doi.org/10.4996/fireecology.1203099

Marsh, C., D. Krofcheck, and M. D. Hurteau. 2022. Identifying microclimate tree seedling refugia in post-wildfire landscapes. *Agricultural and Forest Meteorology* 313 : 108741. https://doi.org/10.1016/j.agrformet.2021.108741.

McCarley, T. R., C. A. Kolden, N. M. Vaillant, A. T. Hudak, A. M. S. Smith, B. M. Wing, B. S. Kellogg, and J. Kreitler. 2017. Multi-temporal LiDAR and Landsat quantification of fire-induced changes to forest structure. *Remote Sensing of Environment* 191:419–432. https://doi.org/10.1016/j.rse.2016.12.022.

Mestre-Runge, C., M. Ludwig, M. T. Sebastià, J. Plaixats, and A. Lobo. 2023. Optimizing Drone-Based Surface Models for Prescribed Fire Monitoring. *Fire* 6:419. https://doi.org/10.3390/fire6110419.

Miller, J. D., E. E. Knapp, C. H. Key, C. N. Skinner, C. J. Isbell, R. M. Creasy, and J. W. Sherlock. 2009. Calibration and validation of the relative differenced Normalized Burn Ratio (RdNBR) to three measures of fire severity in the Sierra Nevada and Klamath Mountains, California, USA. *Remote Sensing of Environment* 113:645–656. https://doi.org/10.1016/j.rse.2008.11.009.

Miller, C. W., B. J. Harvey, V. R. Kane, L. M. Moskal, E. Alvarado, C. W. Miller, B. J. Harvey, V. R. Kane, L. M. Moskal, and E. Alvarado. 2023. Different approaches make comparing studies of burn severity challenging: A review of methods used to link remotely sensed data with the Composite Burn Index. *International Journal of Wildland Fire* 32:449–475. https://doi.org/10.1071/WF22050.

Moran, C. J., V. Hoff, R. A. Parsons, L. P. Queen, and C. A. Seielstad. 2022. Mapping Fine-Scale Crown Scorch in 3D with Remotely Piloted Aircraft Systems. *Fire* 5:59. https://doi.org/10.3390/fire5030059.

Parks, S. A., L. M. Holsinger, M. J. Koontz, L. Collins, E. Whitman, M.-A. Parisien, R. A. Loehman, J. L. Barnes, J.-F. Bourdon, J. Boucher, Y. Boucher, A. C. Caprio, A. Collingwood, R. J. Hall, J. Park, L. B. Saperstein, C. Smetanka, R. J. Smith, and N. Soverel. 2019. Giving Ecological Meaning to Satellite-Derived Fire Severity Metrics across North American Forests. *Remote Sensing* 11:1735. https://doi.org/10.3390/rs11141735.

Parrot. 2016. *Sequoia Datasheet* [WWW Document]. URL https://www.parrot.com/en/support/documentation/sequoia (Accessed 10.5.23).

Perry, D. A., P. F. Hessburg, C. N. Skinner, T. A. Spies, S. L. Stephens, A. H. Taylor, J. F. Franklin, B. McComb, and G. Riegel. 2011. The ecology of mixed severity fire regimes in Washington, Oregon, and Northern California. *Forest Ecology and Management* 262:703–717.

Porcher, R. D., and D. A. Rayner. 2001. *A guide to the wildflowers of South Carolina*. SC: University of South Carolina Press Columbia.

Prošek, J., and P. Šímová. 2019. UAV for mapping shrubland vegetation: Does fusion of spectral and vertical information derived from a single sensor increase the classification accuracy? *International Journal of Applied Earth Observation and Geoinformation* 75:151–162.

Reilly, S., M. L. Clark, L. P. Bentley, C. Matley, E. Piazza, and I. Oliveras Menor. 2021. The Potential of Multispectral Imagery and 3D Point Clouds from Unoccupied Aerial Systems (UAS) for Monitoring Forest Structure and the Impacts of Wildfire in Mediterranean-Climate Forests. *Remote Sensing* 13:3810. https://doi.org/10.3390/rs13193810.

Robinson, J. M., P. A. Harrison, S. Mavoa, and M. F. Breed. 2022. Existing and emerging uses of drones in restoration ecology. *Methods in Ecology and Evolution* 13:1899–1911. https://doi.org/10.1111/2041-210X.13912.

Rothermel, R.C., 1991. Predicting behavior and size of crown fires in the northern Rocky Mountains. Res. Pap. INT-438. Ogden, UT: U.S. Department of Agriculture, Forest Service, Intermountain Research Station. 46 p. 438. https://doi.org/10.2737/INT-RP-438.

Rydgren, K., G. Hestmark, and R. H. Økland. 1998. Revegetation following experimental disturbance in a boreal old-growth *Picea abies* forest. *J Vegetation Science* 9:763–776. https://doi.org/10.2307/3237042.

Saberi, S. J., M. C. Agne, and B. J. Harvey. 2022. Do you CBI what I see? The relationship between the Composite Burn Index and quantitative field measures of burn severity varies across gradients of forest structure. *International Journal of Wildland Fire* 31:112–123.

Samiappan, S., L. Hathcock, G. Turnage, C. McCraine, J. Pitchford, and R. Moorhead. 2019. Remote sensing of wildfire using a small unmanned aerial system: Post-fire mapping, vegetation recovery and damage analysis in Grand Bay, Mississippi/Alabama, USA. *Drones* 3:43.

Sayer, M.A.S., Tyree, M.C., Kuehler, E.A., Jackson, J.K., Dillaway, D.N., 2020. Physiological mechanisms of foliage recovery after spring or fall crown scorch in young longleaf pine (Pinus palustris Mill.). *Forests* 11:208. https://doi.org/10.3390/f11020208.

Scharko, N. K., A. M. Oeck, T. L. Myers, R. G. Tonkyn, C. A. Banach, S. P. Baker, E. N. Lincoln, J. Chong, B. M. Corcoran, and G. M. Burke. 2019. Gas-phase pyrolysis products emitted by prescribed fires in pine forests with a shrub understory in the southeastern United States. *Atmospheric Chemistry and Physics* 19:9681–9698.

Shen, X., L. Cao, B. Yang, Z. Xu, and G. Wang. 2019. Estimation of Forest Structural Attributes Using Spectral Indices and Point Clouds from UAS-Based Multispectral and RGB Imageries. *Remote Sensing* 11:800. https://doi.org/10.3390/rs11070800.

Shin, J., W. Seo, T. Kim, J. Park, and C. Woo. 2019. Using UAV Multispectral Images for Classification of Forest Burn Severity—A Case Study of the 2019 Gangneung Forest Fire. *Forests* 10:1025. https://doi.org/10.3390/f10111025.

Sun, Z., X. Wang, Z. Wang, L. Yang, Y. Xie, and Y. Huang. 2021. UAVs as remote sensing platforms in plant ecology: Review of applications and challenges. *Journal of Plant Ecology* 14:1003–1023.
Swezey, C. S., B. A. Fitzwater, G. R. Whittecar, S. A. Mahan, C. P. Garrity, W. B. Alemán González, and K. M. Dobbs. 2016. The Carolina Sandhills: Quaternary eolian sand sheets and dunes along the updip margin of the Atlantic Coastal Plain province, southeastern United States. *Quaternary Research* 86:271–286. https://doi.org/10.1016/j.yqres.2016.08.007.
Sword, M. A., and J. D. Haywood. 1995. EFFECTS OF CROWN SCORCH ON LONGLEAF PINE FINE ROOTS^1. *General Technical Report Southern Research Station* 1:223.
Szpakowski, D. M., and J. L. Jensen. 2019. A review of the applications of remote sensing in fire ecology. *Remote Sensing* 11:2638.
Viana-Soto, A., M. García, I. Aguado, and J. Salas. 2022. Assessing post-fire forest structure recovery by combining LiDAR data and Landsat time series in Mediterranean pine forests. *International Journal of Applied Earth Observation and Geoinformation* 108 : 102754.
Wade, D.D., Johansen, R.W., 1986. Effects of Fire on Southern Pine: Observations and Recommendations. Gen. Tech. Rep. SE-41. Asheville, NC: U.S. Department of Agriculture, Forest Service, Southeastern Forest Experiment Station. 14 p. 041. https://doi.org/10.2737/SE-GTR-41
Wagner, C. E. V. 1977. Conditions for the start and spread of crown fire. *Canadian Journal of Forest Research* 7:23–34. https://doi.org/10.1139/x77-004.
Weise, D.R., Wade, D.D., Johansen, R.W., Preisler, H.K., Combs, D.C., Ach, E.E., 2016. Defoliation effects on growth and mortality of three young southern pine species. Res. Pap. PSW-RP-267. Albany, CA: U.S. Department of Agriculture, Forest Service, Pacific Southwest Research Station. 70 p 267. https://doi.org/10.2737/PSW-RP-267.
Weise, D.R., Fletcher, T.H., Johnson, T.J., Hao, W.M., Dietenberger, M., Princevac, M., Butler, B.W., McAllister, S.S., O'Brien, J.J., Louise Loudermilk, E., Ottmar, R.D., Hudak, A.T., Kato, A., Shotorban, B., Mahalingam, S., Myers, T.L., Palarea-Albaladejo, J., Baker, S.P., 2024. Comparing gas composition from fast pyrolysis of live foliage measured in bench-scale and fire-scale experiments. Int. J. Wildland Fire 16. https://doi.org/10.1071/WF23200
Weise, D.R., Hao, W.M., Baker, S., Lincoln, E., Hudak, A.T., Bright, B.C., Princevac, M., Aminfar, A., Ottmar, R.D., O'Brien, J.J., Kato, A., Batchelor, J.L., Herzog, M.M., Chong, J., Corcoran, B.M., Burke, G.M., 2025. Pyrolysis gases measured by gas chromatography and mass spectrometry from fires in a wind tunnel and at Ft. Jackson, SC. https://doi.org/10.60594/W48G6B
Westoby, M. J., J. Brasington, N. F. Glasser, M. J. Hambrey, and J. M. Reynolds. 2012. 'Structure-from-Motion' photogrammetry: A low-cost, effective tool for geoscience applications. *Geomorphology* 179:300–314. https://doi.org/10.1016/j.geomorph.2012.08.021.
White, J. D., K. C. Ryan, C. C. Key, and S. W. Running. 1996. Remote Sensing of Forest Fire Severity and Vegetation Recovery. *International Journal of Wildland Fire* 6:125–136. https://doi.org/10.1071/wf9960125.
Wright, C. S., and J. K. Agee. 2004. Fire and Vegetation History in the Eastern Cascade Mountains, Washington. *Ecological Applications* 14:443–459. https://doi.org/10.1890/02-5349.
Yin, T., P. M. Montesano, B. D. Cook, E. Chavanon, C. S. R. Neigh, D. Shean, D. Peng, N. Lauret, A. Mkaouar, D. C. Morton, O. Regaieg, Z. Zhen, and J.-P. Gastellu-Etchegorry. 2023. Modeling forest canopy surface retrievals using very high-resolution spaceborne stereogrammetry: (I) methods and comparisons with actual data. *Remote Sensing of Environment* 298 : 113825. https://doi.org/10.1016/j.rse.2023.113825.
Zar, J.H., 1974. Biostatistical analysis, Prentice-Hall biological sciences series. Prentice-Hall, Englewood Cliffs, N.J. 620 p.

Publisher's Note